Received: 29 September 2022 | Revised: 23 January 2023 | Accepted: 22 February 2023

DOI: 10.1111/jace.19085

Journal of the American Ceramic Society

RESEARCH ARTICLE

Manufacturing and deformation behavior of alumina and zirconia helical springs at room temperature

Torsten Rabe | **Gerhard Kalinka** | **Björn Mieller**

Department Materials Engineering, Federal Institute for Materials Research and Testing BAM, Berlin, Germany

Correspondence
Björn Mieller, Department Materials Engineering, Federal Institute for Materials Research and Testing BAM, Unter den Eichen 44-46, 12200 Berlin, Germany.
Email: bjoern.mieller@bam.de

Funding information
Bundesministerium für Bildung und Forschung, Grant/Award Number: 13XP5006D

Abstract

Ceramic helical springs with identical dimensions were produced by hard machining from alumina, alumina toughened zirconia (ATZ), and tetragonal zirconia polycrystals (TZP) stabilized with different oxides. According to the results of the spring constant determination under deformation rates of 3 mm/min, the deformation behavior of all ceramic springs obeys to Hook's law. However, variation of the deformation rate, tests under constant load, and spring recovery behavior revealed differences in the deformation behavior of alumina, TZP, and ATZ springs. Alumina springs exhibited time-independent deformation in all tests. In contrast, anelastic deformation at room temperature was demonstrated in all springs containing TZP. This deformation is completely reversible over a period of several days. Anelastic behavior is particularly pronounced in Y-TZP springs, whereas Ce-TZP springs exhibit comparatively very low but still reliably detectable anelasticity. Oxygen vacancies in the TZP ceramic are considered the most likely explanation for the anelastic behavior of TZP springs at room temperature.

KEYWORDS
alumina, creep, elastic materials/properties, zirconia: yttria stabilized

1 | INTRODUCTION

There is a need for springs in harsh working conditions such as at high temperature, high wear, or high corrosion rates. Ceramics have this potential due to their promising combination of chemical, thermal, and mechanical properties. Ceramic materials have better corrosion and wear resistances compared to other potential spring materials. In addition, unlike metallic springs, ceramic springs retain their elasticity at higher temperatures. Ceramic springs can be used at temperatures up to about 1000°C, as shown for springs made of alumina[1] and silicon nitride.[2] Decisive factors for the choice of ceramic springs can also be lower mass, lower thermal and electrical conductivity, and inert behavior in magnetic fields.

Ceramic springs have been tested for a variety of applications, some of which are used industrially. Harper[1] designed and manufactured alumina seat preloading springs for use in high-temperature coal gasification valves. Grujicic[3] identified ceramic matrix composites as particularly suitable for clamping springs in industrial gas turbine engines. Furthermore, ceramic springs have been tested and used so far, for example, as valve springs,[4] as high-temperature components in vacuum tubes and

relays,[5] in semiconductor production,[6–8] and in magnetic resonance imaging scanners. In recent years, the increase of efficiency in mechanical systems has become more important, and this has led to a demand for springs with smaller energy losses in the application.[9] Hereby, the spring material should have a low loss coefficient. This is the fraction of mechanical energy loss in a stress–strain cycle and an important dimensionless material parameter in cyclic loading. Advanced ceramics have the lowest loss coefficient with a four-order-of-magnitude reduction compared to elastomers. Moreover, high-carbon steels have a higher loss coefficient than ceramic materials.

Despite the advantageous properties of ceramics, limited reliability and high production costs are obstacles to wider use of ceramic springs. Therefore, several ceramic forming processes have been tested to minimize microstructure and surface defects as well as to reduce production costs. As the first mention of ceramic helical springs made of sintered glass-bonded alumina by Rudolph in 1961,[5] various ceramic shaping technologies for helical springs have been developed. A summary on the literature on extrusion, injection molding, and gel casting for spring fabrication is provided as SM1. Another technique for the production of ceramic springs is the mechanical processing of isostatically pressed hollow cylinders.[4] A combination of cutting spring coils into the green or partially sintered hollow cylinder and fine grinding of the coil surfaces after dense sintering is often used.[1,10,11] Time-consuming and costly hard machining of sintered cylinders or springs is unavoidable when springs with tight dimensional tolerances and good surface quality are required. Hard machining allows for various spring designs with respect to inner and outer diameter, spring length, pitch, and coil spacing. However, only a rectangular cross section of the coil is possible when hard machining is used.

The literature reports the realization of springs from numerous structural ceramics. In addition to high-strength oxide materials, such as alumina,[5,12–14] alumina toughened zirconia (ATZ),[11] zirconia toughened alumina,[15] tetragonal zirconia polycrystals (TZP),[12] and partially stabilized zirconia (PSZ),[4,11] the spectrum of materials also includes silicon nitride[2,10,11] and graphite.[7] Great potential is seen for springs made of ceramic composites such as C/SiC[16] and multi-composites containing mullite, SiC particles, and SiC whiskers.[17]

An innovative application of ceramic springs was recently proposed by the authors of this article and realized in a research project. A capacitive force sensor based on ceramic springs with metallized coils was developed. The prerequisite for high resolution capacitive spring sensors is a linear stress–strain behavior of the springs independent of load speed and load time. For ceramic springs, a linear stress–deformation behavior is usually assumed. Several publications have postulated, based on stress–strain measurements, that ceramic helical springs obey Hooke's law at room temperature over wide load ranges. Hamilton[4] found a corresponding behavior for helical springs made of partially stabilized zirconia (MgO–PSZ) by hard machining, Krindges[12] for injection molded springs made of alumina and zirconia (Y-TZP), and Zhuang[18] for helical springs made of Y-TZP produced by gel casting. In the high-temperature range above 800°C, however, deviations from linear stress–strain behavior were measured on Y-TZP springs, as expected. Nonelastic behavior occurred and the energy loss increased.[18]

Long-term stable springs with perfect elastic behavior under static and dynamic loading conditions are required for capacitive spring sensors. It was estimated that the results on the stress–strain behavior of ceramic springs available in the literature so far are not sufficient to reliably assess their suitability for capacitive spring sensors. Therefore, high-quality helical springs with defined geometry were produced by hard machining of sintered hollow cylinders made of alumina, ATZ, or TZP materials with optimized microstructure. The spring constants as a function of the ceramic material and the deformation rate as well as the deformation of the springs under constant long-term load and the spring recovery behavior were measured with high precision. The aim of these investigations is to prove that these ceramic springs do not exhibit any plastic or anelastic deformation under load in the room-temperature range.

2 | MATERIALS AND METHODS

2.1 | Spring fabrication

Commercially available spray dried granules were used as starting material for the spring production. Table 1 lists the manufacturers and designations of the granules as well as the chemical compositions and granulometric properties of the starting powders. A comprehensive description of the preparation and characterization of the materials is provided as SM2.

Ceramic helical springs were produced in a multistage manufacturing process. First, hollow cylinders were formed by cold isostatic pressing. Then, taking sintering shrinkage into account, the outer and inner diameters as well as the length of the pressed hollow cylinders were adjusted by green machining. After debindering, the hollow cylinders were sintered (chamber furnace 180/08, Ceramics GmbH, Aachen, Germany). The material-specific manufacturing parameters isostatic pressure, maximum sintering temperature, and dwell time are also listed in Table 1.

TABLE 1 Starting powders and processing parameters.

	Alumina	ATZ	3Y-TZP	2Y-TZP	Ce-TZP	Y-Ce-TZP
Manufacturer	PENGDA (China)	Saint-Gobain (France)	TOSOH (Japan)	INNOVNANO (Portugal)	Daiichi Sankyo (Japan)	TOSOH + Daiichi Sankyo
Designation	PG 4N25M	UprYZe shock G	TZ-3YSB-E	2YSZ	CEZ 12-2	TZ-3YSB-E + CEZ 12-2
Chemical composition[a] in wt.%	99.99 Al_2O_3	ZrO_2, stabilized with 6.3 (Y_2O_3 + CeO_2) + 15.4 Al_2O_3	ZrO_2, stabilized with 5.2 Y_2O_3 + 0.25 Al_2O_3	ZrO_2, stabilized with 3.4 Y_2O_3 + 0.3 Al_2O_3	ZrO_2, stabilized with 16 CeO_2 + 0.25 Al_2O_3	95.2 3Y-TZP + 4.8 Ce-TZP
Specific surface in m^2/g	8.0[b]	8.2[a]	9[a]	13.1[b]	13.00[b]	n.d.
Mean particle size d_{50} in μm	0.25[a]	0.20[a]	0.09[a]	0.22[a]	0.45[b]	n.d.
Isostatic pressure in MPa	200	135	135	200	135	135
Sintering temperature in °C	1500	1450	1470	1370	1470	1470
Dwell time in h	3	2	2	4	2	2

[a]Manufacturer information.

[b]Determination at BAM n.d.—not determined.

Abbreviations: ATZ, alumina toughened zirconia; TZP, tetragonal zirconia polycrystals.

After sintering, the hollow cylinders were hard machined to precisely set specified inner and outer diameters and reduce surface roughness. First, the inner surfaces were pre-ground and then honed. Then the outsides of the hollow cylinders were machined with grinding wheels. The spring coils were produced by multistage hard machining the hollow cylinders on the 5-axis DMU 65 Ultrasonic milling machine (DMG Mori, Wernau, Germany), see Figure 1A. The hollow cylinders were fixed with hot-melt adhesive (Crystalbond 509-1, Aremco Products Inc., USA) on a custom-made metallic workpiece carrier (Figure 1B), which was clamped and aligned in the milling machine. To reduce the processing temperatures during the milling of the spring coils, coolable grinding wheel supports were developed and used (Figure 1C).

The groove was milled in the fixed hollow cylinder using a metal-bonded diamond wheel (grit D46, width 0.45 mm), with the tool rotating at 12 500 rpm and the workpiece spindle at 1 rpm in the same direction. The maximum feed was limited to 0.5 mm to avoid chipping. Due to the hollow cylinder wall thickness of 1.75 mm, four milling steps were necessary. A finer metal-bonded diamond wheel (D30, width 0.5 mm) was used to finish the coil surfaces. For producing helical springs with flat ends, the spring is then cut to the desired length. Cuts are made at right angles to the hollow cylinder axis. The workpiece carrier with the glued-on ceramic spring was heated to 90°C to soften the adhesive and allow the spring to be drawn off the workpiece carrier. The spring was then ultrasonically cleaned in an acetone bath to completely remove the adhesive residues.

If the described process technology is carefully executed, the coil width and height can be realized with a manufacturing tolerance of ±10 μm. Helical ceramic springs could be manufactured with a well reproducible spring constant (scatter in the range of only ±1%), with low coil surface roughness of $R_a < 0.2$ μm and without edge chipping.

2.1.1 | Helical springs with flat ends

To investigate the effect of deformation rate on spring constant and spring deformation behavior at constant load, helical springs with rectangular cross section and flat ends were fabricated from alumina, ATZ, 3Y-TZP, 2Y-TZP, and Ce-TZP. The design drawing for this type of spring is shown in Figure 1D. The height of the last upper and lower coils was continuously reduced in the manufacturing process from the initial height of 1 mm down to about 10 μm at the ends of the spring to make the force transmission more uniform under compressive loading. Information on typical spring dimensions used in deformation experiments is given in Table 2. Figure 2A presents springs manufactured from different ceramic materials. All springs have identical dimensions. Characteristic colors after sintering are visible.

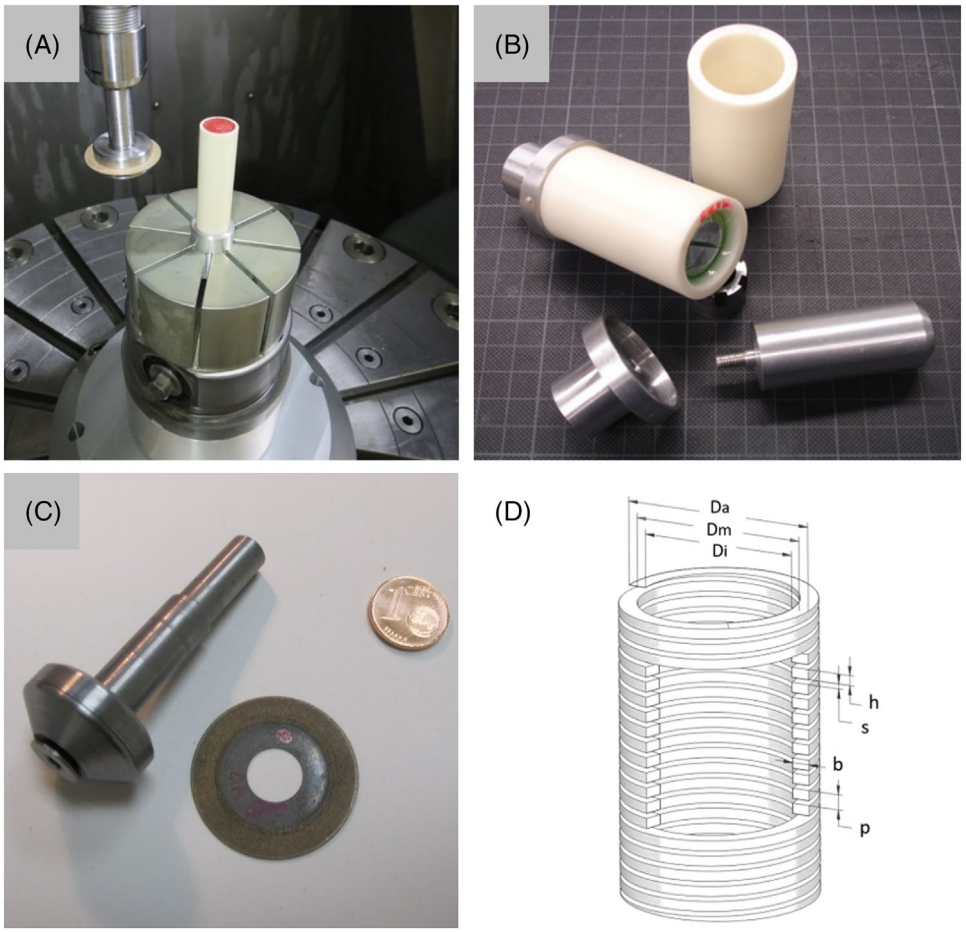

FIGURE 1 Fabrication of ceramic helical springs: (A) rotating milling disk and workpiece spindle with hollow cylinder; (B) workpiece carrier with bonded ceramic hollow cylinder; (C) grinding wheel holder and milling disk; and (d) design drawing of helical spring with flat ends, including designation of dimensioning.

TABLE 2 Dimensions of helical test springs.

Spring dimension	Abbreviation	Helical spring with flat ends	Helical springs with unslotted cylinder ends
Outer spring diameter in mm	D_a	19.03	19.02
Inner spring diameter in mm	D_i	15.48	15.47
Mean spring diameter in mm	D_m	17.25	17.25
Coil width in mm	b	1.78	1.78
Coil height in mm	h	1.00	1.00
Coil spacing in mm	s	0.50	0.52
Pitch in mm	p	1.50	1.52
Total number of coils	i_g	21.5	24

2.1.2 | Helical springs with unslotted cylinder ends

Spring recovery after unloading was investigated on helical spring with unslotted cylindrical ends, which are shown in Figure 2B. This spring is identical to the springs with flat ends in terms of diameter, coil cross section, and spring pitch (Table 2). However, there are differences in the number of coils and the design of the coil ends. The coil height at the spring ends does not become flatter but remains constant. The end of the coils passes directly into the bulk part of the hollow cylinder. To avoid stress peaks at the end of the coil spacing, the cuts end in elongated holes. The spring and the unslotted hollow cylinder sections at the ends form

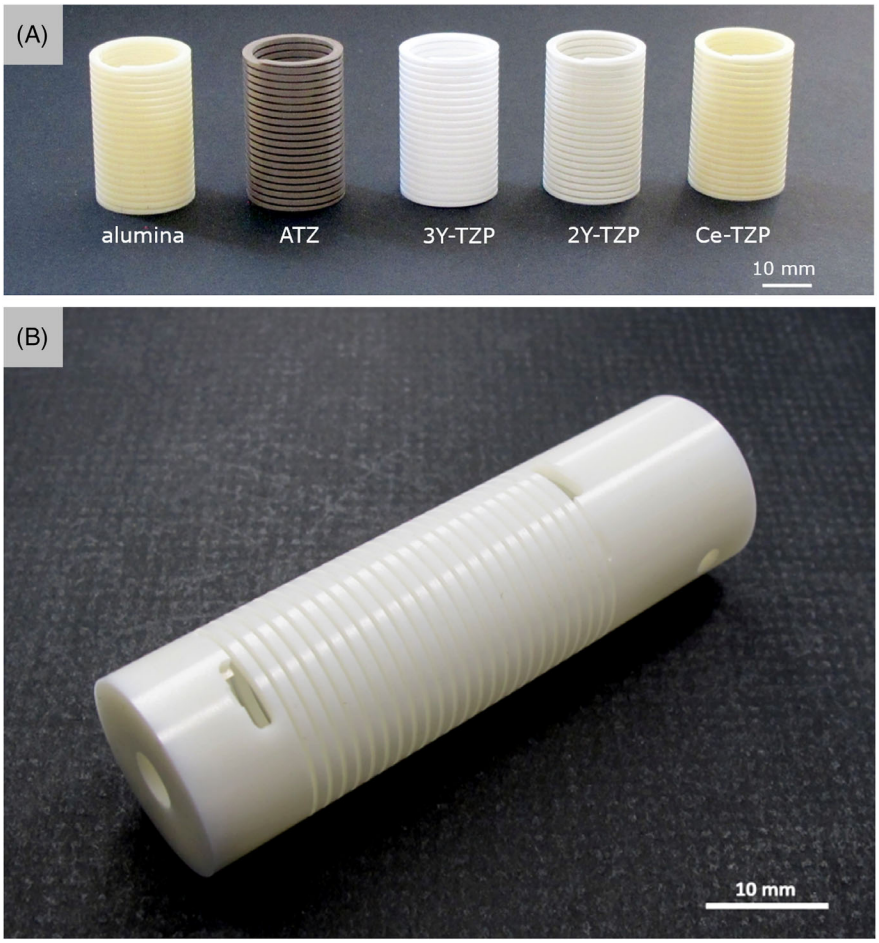

FIGURE 2 (A) Helical springs with flat ends and (B) helical spring with unslotted cylinder ends made from Y-Ce-TZP.

a monolithic component. The hard machining technology developed permits variable design of the spring ends. As a result, the ceramic springs can be integrated into sensor systems and used in a variety of ways in mechanical and plant engineering. Figure 2B shows a TZP spring with spring ends developed for the mounting of a spring sensor. Such a spring design permits the cylindrical spring to be also exposed to tensile loading.

2.2 | Characterization of spring deformation

The deformation of the ceramic springs was studied under different deformation rates, under static loading, and after unloading.

2.2.1 | Spring constants under different deformation rates

Spring constants were determined using the Z2.5/TN1S materials testing machine (ZwickRoell GmbH & Co. KG, Ulm, Germany) shown in Figure 3A. The spring was clamped between two plane-parallel plates, preloaded with a small contact force of about 0.05 N, and compressed at constant speed up to a maximum spring deflection of 3 mm. Spring deformation was controlled using a mechanical displacement measurement system in the crosshead. The force was measured by means a 50 N load cell. Force and deformation were recorded at a constant sampling rate of 50 Hz. Five measurements were made on each of the springs with the same position of the coil ends, with a time interval of 30 min between each measurement. The average spring constants with standard deviation were calculated from the results of the five individual measurements.

In further tests, the deformation rates were varied. In addition to the measurement at 3 mm/min, the spring constants were also determined at deformation rates of 0.1, 1, 10, and 30 mm/min.

2.2.2 | Deformation under static loading

A special test rig was developed to investigate the deformation stability of helical springs under constant load. This was used to track changes in the length of the springs in the

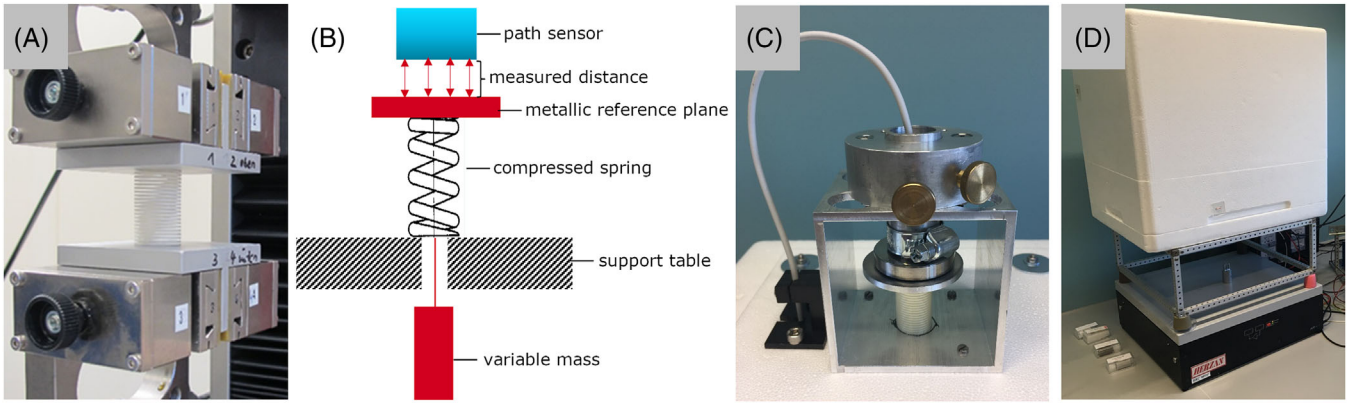

FIGURE 3 (A) Test setup for determination of spring constant with clamped spring, (B) schematic drawing of test setup for the determination of deformation under static load, (C) static load test setup with clamped spring, reference plate and sensor unit, and (D) exterior view of the test rig with thermo-isolation chamber and vibration damper.

micrometer range over several hours. The measuring principle is based on the change in capacitance as a response to a distance change between a reference plate and the displacement sensor (Figure 3B). The measuring setup with compressed ceramic spring, reference plate, and capacitive displacement sensor with a working range of 7 mm and a local resolution of 10 nm is shown in Figure 3C. To minimize temperature fluctuations on the sample during the measurement, spring and sensor are surrounded by a heated, double-layered polystyrene box with integrated temperature sensors (Figure 3D). The temperature is thereby kept constant at ±0.02 K over a period of several days. The measuring device was placed on a vibration-damped table to minimize falsification of the measured values by vibrations.

The measurement routine starts with the installation of the spring, where the spring is preloaded by the weight of the reference plate with the hook for hanging the variable test weight. To ensure a constant temperature of 26.5°C inside the measuring chamber, a preheating period of 4 h was applied. Then a defined mass of 50 g was attached to the reference plate, and after 10 s, the measurement was started. The changes in the distance between the reference plate and the sensor, and thus the deformation of the spring, as well as the temperature at the spring were recorded at a frequency of 10 Hz.

2.2.3 | Spring recovery after unloading

The time course of spring relaxation after unloading was investigated on springs with unslotted cylinder ends. First, all coil distances along a marked line were measured on the unloaded spring using a ScopeCheck 300 coordinate measuring machine (Werth Messtechnik GmbH, Giessen, Germany). Subsequently, the coil spacing of the spring was reduced to approx. 10%. The force required for this was kept constant for several days. Immediately after the spring was unloaded, the coil distances along the marked line were again determined using the coordinate measuring machine. Further distance measurements were carried out after 20 min, 5, 24, and 144 h.

3 | RESULTS

The results of microstructural and mechanical characterization of the spring materials are provided as SM3 and SM4, respectively.

3.1 | Material dependence of spring constant

In Table 3, the mean spring constants with the standard deviation calculated from the results of the five individual measurements are documented. The corresponding force–displacement curves are shown in Figure 4A. Low standard deviations between 0.04% and 0.15% prove a good repeatability of the measurement results on all springs. The spring constant of alumina is about twice that of the TZP materials, and this means the alumina spring is significantly stiffer. Springs made of the two Y-TZP materials have almost identical spring constants, whereas the Ce-TZP spring is slightly softer. When the composite material ATZ is used, the spring constant is determined by the volume fractions of 3Y-TZP and alumina. Consequently, ATZ springs with 15.4 wt.% alumina have a slightly higher spring constant than those made from single-phase TZP materials.

Table 3 also shows the mean fitting standard errors averaged from the results of each of five repeat measurements

TABLE 3 Spring constants at loading rate of 3 mm/min.

Spring material	Mean spring constant K in N/mm	Standard deviation in N/mm and %		Mean fit standard error in N/mm
Alumina	0.7460	0.0003	0.043	0.000038
ATZ	0.4358	0.0005	0.125	0.000026
3Y-TZP	0.3603	0.0003	0.079	0.000028
2Y-TZP	0.3576	0.0005	0.151	0.000040
Ce-TZP	0.3397	0.0004	0.110	0.000022

Abbreviations: ATZ, alumina toughened zirconia; TZP, tetragonal zirconia polycrystals.

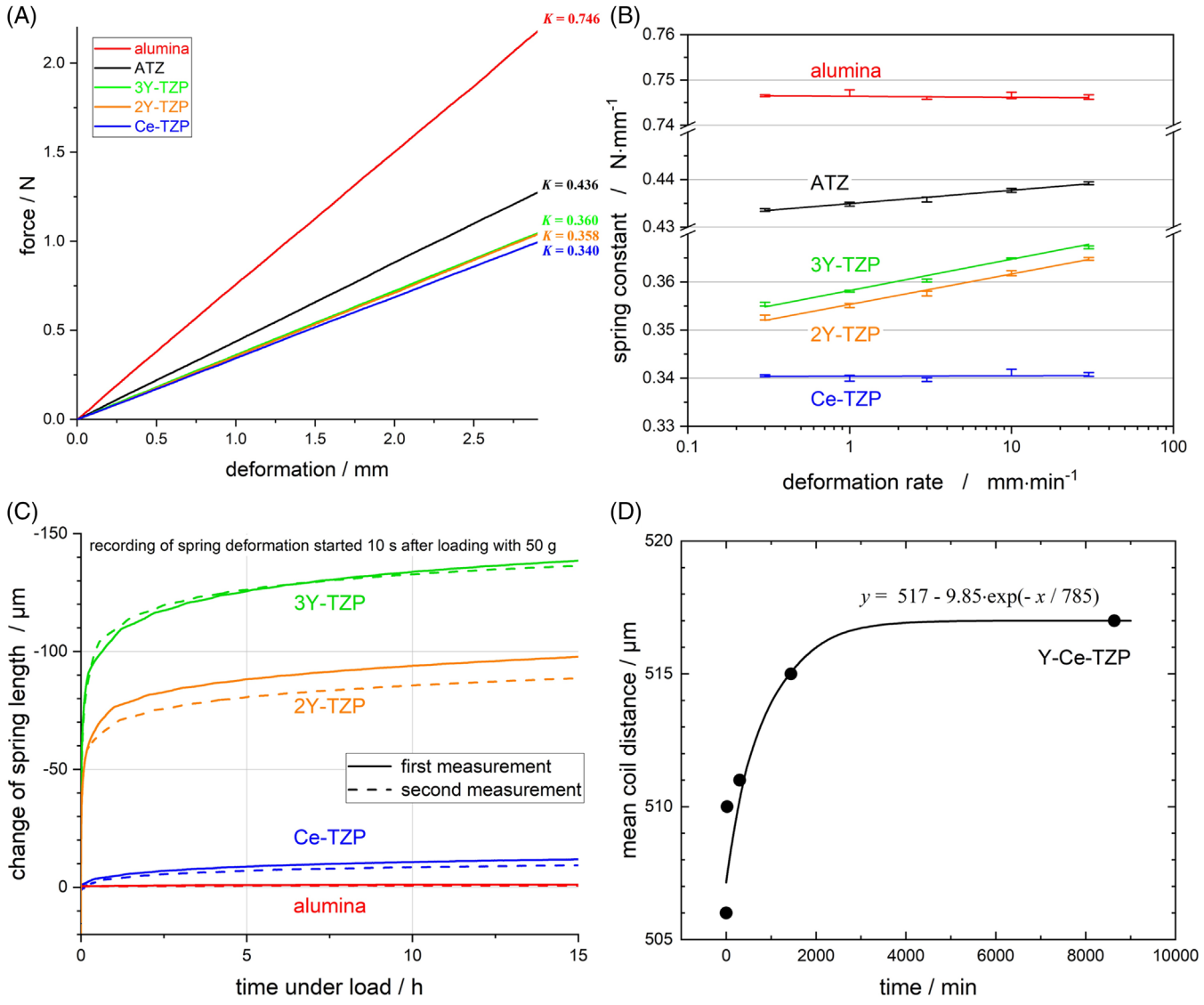

FIGURE 4 Results of spring characterization: (A) force–deformation curves at deformation rate of 3 mm/min; (B) influence of the deformation rate on the spring constant, error bars represent double standard deviation of five repeat measurements; (C) change of spring length under constant compressive load; and (D) time dependence of spring relaxation after unloading, dots: measured values, line: exponential function as guide for the eye.

TABLE 4 Calculated shear moduli and shear stresses.

Spring material	Calculated shear modulus G in GPa	Required force F at spring deflection of 3 mm in N	Shear stress τ at spring deflection of 3 mm in MPa
Alumina	151.1	2.24	45.1
ATZ	88.3	1.31	26.4
3Y-TZP	72.4	1.08	21.8
2Y-TZP	72.5	1.07	21.6
Ce-TZP	68.8	1.02	20.5

Abbreviations: ATZ, alumina toughened zirconia; TZP, tetragonal zirconia polycrystals.

in each case. The fitting error describes the deviation of the measuring curve from the regression line determined by the least squares method. The fitting error as a measure of the linearity deviation is very small for all springs investigated. The results of the spring constant determination at constant deformation rate of 3 mm/min demonstrate a strictly linear relationship between applied force and deformation for alumina, TZP, and ATZ springs.

According to Equation (1), the spring constant K of coil springs depends on the shear modulus G, the coil cross section (width b, height h), the mean coil diameter D_m, the number of active coils n, and the coefficient ε, which is determined by the ratio b/h and can be taken from a table in Ref. [19]:

$$K = \frac{G \cdot b^2 \cdot h^2}{D_m^3 \cdot n \cdot \varepsilon} \quad (1)$$

Using the experimentally determined spring constant in Table 3 and the spring dimensions (Table 2), the shear moduli of the spring materials were calculated. As the dimensions of all springs are identical, the spring constant is directly proportional to the shear modulus of the ceramic and the differences in the spring constants documented in Table 4 are determined only by the type of ceramic material.

Compression causes shear stresses in the ceramic coils of the helical spring. Shear stress τ can be calculated according to the following equation[19]:

$$\tau = \frac{\Psi \cdot D_m}{b \cdot h \cdot \sqrt{b \cdot h}} \cdot F \quad (2)$$

In addition to the spring dimensions, the applied force F and the stress coefficient Ψ must be known. The latter depends on the ratio b/h and can be taken from a graph in Ref. [19]. Table 4 lists the calculated shear stresses generated in the spring coils at a spring deflection of 3 mm. In all five materials, the shear stress is less than 50 MPa. Compared with the fracture stress of the ceramic materials used (Table S5), the stress built up during spring loading is low, and failure of the spring under this loading scenario is unlikely.

3.2 | Deformation rate dependence of spring constant

The spring constants of the alumina, ATZ, 3Y-TZP, 2Y-TZP, and Ce-TZP springs were additionally determined at deformation rates of 0.3, 1, 10, and 30 mm/min. Figure 4B illustrates the material-specific dependence of the spring constant on the deformation rate. Table 5 summarizes the spring constants averaged from five measurements each with standard deviation as well as the results of the regression analyses.

The differences of mean values of spring constant at different deformation rates were tested with pairwise t-test at a significance level of 0.95. Significant differences of mean value are indicated by a p-value <.05. The spring constant of alumina springs is independent of the deformation rate ($p > .1$). The differences in the spring constant at different deformation rates are within the range of the measurement accuracy of the test method. For the Ce-TZP spring, no dependence of the spring constant on the deformation rate was found either ($p > .1$). In contrast, the measured spring constant of the 3Y-TZP spring rises continuously with increasing deformation rate ($p < 4 \times 10^{-7}$). The spring constant grows by 3.3% when the deformation rate is changed from 0.3 to 30 mm/min. A similar behavior is also observed for 2Y-TZP springs ($p < 1 \times 10^{-5}$). Here, the spring constant increases by 3.5%. For springs made of ATZ, a composite of 3Y-TZP, and alumina, the dependence of the spring constant on the deformation rate is lower than for springs made of single-phase Y-TZP materials. However, a significant difference was also demonstrated for this composite material ($p < 4 \times 10^{-3}$). The increase in spring constant here was 1.3%.

The variations in measured values among the five repeat measurements in each case are visualized by bars in the size of twice the standard deviations. Furthermore, the calculated regression lines are plotted in the diagram (Figure 4B). An increase of the spring constant with increasing deformation rate is clearly visible for the ATZ spring and especially for the 3Y-TZP and 2Y-TZP springs. The calculated slope of the regression line for both the alumina spring and the Ce-TZP spring is very small. At

TABLE 5 Influence of deformation rate on spring constant.

Spring material	Deformation rate in mm/min	Mean spring constant in N/mm	Standard deviation in N/mm	%	Slope of regression line	Fit standard error	Change of spring constant[a] in %
Alumina	0.3	0.7465	2.0×10^{-4}	0.022	-2.10×10^{-4}	2.0×10^{-4}	−0.04
	1	0.7471	7.0×10^{-4}	0.090			
	3	0.7460	3.0×10^{-4}	0.043			
	10	0.7466	7.0×10^{-4}	0.098			
	30	0.7462	5.0×10^{-4}	0.073			
ATZ	0.3	0.4336	3.0×10^{-4}	0.125	2.81×10^{-3}	1.3×10^{-4}	+1.29
	1	0.4348	4.0×10^{-4}	0.090			
	3	0.4358	5.0×10^{-4}	0.125			
	10	0.4377	4.0×10^{-4}	0.101			
	30	0.4392	3.0×10^{-4}	0.066			
3Y-TZP	0.3	0.3554	4.0×10^{-4}	0.111	6.51×10^{-3}	4.4×10^{-4}	+3.32
	1	0.3581	2.0×10^{-4}	0.054			
	3	0.3603	3.0×10^{-4}	0.079			
	10	0.3649	1.0×10^{-4}	0.021			
	30	0.3672	3.0×10^{-4}	0.070			
2Y-TZP	0.3	0.3526	5.0×10^{-4}	0.147	6.33×10^{-3}	2.9×10^{-4}	+3.46
	1	0.3551	4.0×10^{-4}	0.118			
	3	0.3576	5.0×10^{-4}	0.151			
	10	0.3618	5.0×10^{-4}	0.141			
	30	0.3648	3.0×10^{-4}	0.083			
Ce-TZP	0.3	0.3405	2.0×10^{-4}	0.060	8.0×10^{-5}	2.9×10^{-4}	+0.09
	1	0.3400	6.0×10^{-4}	0.189			
	3	0.3397	4.0×10^{-4}	0.110			
	10	0.3412	7.0×10^{-4}	0.196			
	30	0.3408	4.0×10^{-4}	0.126			

[a]Change of the spring constant when increasing the deformation rate from 0.3 to 30 mm/min.

Abbreviations: ATZ, alumina toughened zirconia; TZP, tetragonal zirconia polycrystals.

this point, it should be noted that Equation (1) does not account for deformation rate dependence. As the absolute change of the spring constant with the deformation rate is small, Equation (1) can certainly be applied to the design of helical ceramic compression springs.

3.3 | Spring deformation under constant load

The time-dependent deformation of alumina, Ce-TZP, 2Y-TZP, and 3Y-TZP springs is shown in Figure 4C. Alumina and TZP springs react differently to static compressive loading. The length of the alumina spring remains stable throughout the measurement period. In contrast, the length of the Y-TZP springs decreases significantly, that is, the spring deformation increases, especially in the first hour after the start of loading. During the entire loading period of 15 h, the change in the length of 2Y-TZP and 3Y-TZP springs was about 100 and 140 μm, respectively. For the Ce-TZP spring, the increase in deformation was much smaller, but still clearly measurable. This spring was compressed by about 10 μm in 15 h. Thus, this experimental result proves that not only Y-TZP and ATZ springs but also Ce-TZP springs exhibit time-dependent deformation behavior.

The curves progression indicates that the deformation of all TZP springs is not yet completed even after 15 h. Repeated measurements of 3Y-TZP and Ce-TZP springs showed a good reproducibility of the results, provided that the repeated measurements were started after the spring recovery had been completed. Figure 4C shows that the curves of the first and the second measurement performed 8 days later are almost congruent for the 3Y-TZP and the Ce-TZP spring. A smaller deformation was measured for the 2Y-TZP spring during the second measurement. As this spring was only stored load-free for 1 day before the second measurement, recovery was probably not yet complete.

TABLE 6 Time-dependent changes of coil distances after unloading of Y-Ce-TZP spring.

Time of measurement	Mean coil distance s in μm	Change of mean coil distance in %	Minimum coil distance s_{min} in μm	Maximum coil distance s_{max} in μm	s_{max}–s_{min} in μm
Before spring loading	517	0	509	525	16
Immediately after spring unloading	506	−2.1	498	514	16
20 min after spring unloading	510	−1.4	501	518	17
5 h after spring unloading	511	−1.2	503	519	16
24 h after spring unloading	515	−0.4	507	522	15
144 h after spring unloading	517	0	509	524	15

3.4 | Spring recovery behavior

The coil distances of the Y-Ce-TZP spring shown in Figure 2B were measured with a coordinate measuring machine before the spring was compressed. In this initial state, the coil distances vary between 509 and 525 μm. These differences result from the multistage hard machining process used to cut the coil spacings into the sintered hollow cylinders. It should be noted, however, that the realizable tolerances of the coil spacing are much larger for injection-molded or extruded springs.

After several days of compression, the spring was unloaded, and the coil distances were measured immediately, after 20 min, and after 5, 24, and 144 h. In Figure S6, the measured values for every winding and time are plotted. Table 6 shows the average coil spacings calculated from the 22 coil spacings before loading and at various times after unloading. Immediately after spring unloading, the mean spring distances are 2.1% less than before spring loading. In addition, Table 6 lists the respective minimum and maximum coil spacings. The smallest values were always determined for coil spacing number 11, and the largest values for coil spacing number 21 (see Figure S6). The difference between minimum and maximum coil distances was almost constant at all measurement times.

Immediately after spring unloading, coil spacings are approx. 10 μm smaller than before compression loading. Subsequently, the coil distances gradually approach the initial values. But even 24 h after the spring has been unloaded, spring recovery is not yet finished. A small but reliably detectable difference of about 2 μm remains. Only a further measurement of the coil distances after 144 h showed that it largely matched the measured values before spring compression.

To visualize this behavior, the mean coil distance is plotted in dependence of time after unloading in Figure 4D. An exponential function that implies time-dependent anelastic behavior is also shown for comparison.

Analogous investigations were also carried out on alumina springs. In contrast to the Y-Ce-TZP spring, alumina springs exhibit an immediate complete strain recovery after unloading.

4 | DISCUSSION

4.1 | Comparison and evaluation of spring materials

Ceramic helical springs were produced from four materials with single-phase microstructure (alumina, 3Y-TZP, 2Y-TZP, and Ce-TZP) and two ceramic composites (ATZ and Y-Ce-TZP) by hard machining of hollow cylinders. Coil width and height were realized with a manufacturing tolerance of ±10 μm. With this technology, helical springs with well reproducible spring constants, with a low coil surface roughness of $R_a < 0.2$ μm and without edge chipping, can be produced. The microstructure and mechanical properties of the materials used for spring production (Table S5) correspond to the requirements demanded of high-quality materials made of alumina, ATZ, and TZP. This ensures that the analyzed deformation behavior of the springs is representative for the respective ceramic type. From the deformation tests, the following conclusions can be drawn about the behavior of helical springs made of alumina, ATZ, and TZP at room temperature:

Alumina springs showed a time-independent deformation both in tests with different deformation rates and under static loading as well as after unloading. This corresponds to the behavior generally expected from ceramic materials. Alumina springs thus meet the requirements for use in high-resolution sensor systems.

Higher deformation rates lead to an increase in the spring constant for Y-TZP springs. Under constant loading, spring deformation was shown to progress over several days at room temperature. The deformation process is reversible, but complete recovery requires several days. The 3Y-TZP and 2Y-TZP materials used for spring manufacturing have very different fracture toughness (Table S5). Nevertheless, the corresponding springs behave almost

identically under load. The very good mechanical properties predestine Y-TZP materials to produce reliable and damage-tolerant helical springs. However, due to their time-dependent deformation behavior, Y-TZP springs are unsuitable for the sensor application described.

ATZ springs with 85 wt.% Y-TZP also show anelastic behavior in the load tests, but this is less pronounced compared to springs made of pure Y-TZP. The addition of approx. 15 wt.% alumina particles and platelets to the Y-TZP matrix reduces the anelastic behavior more than was to be expected based on the volume fraction.

Different deformation experiments on Ce-TZP springs gave seemingly contradictory results. The spring constant of Ce-TZP springs, unlike that of Y-TZP springs, did not change significantly when the deformation rate was varied between 0.3 and 30 mm/min. However, in long-term tests under constant load, anelastic deformation was also observed on Ce-TZP springs. Still, this is an order of magnitude smaller than that of Y-TZP springs. It is a fact that Ce-TZP springs exhibit anelastic behavior. Consequently, an increasing loading rate should also result in an increased spring constant. This increase in spring constant is presumably less than the repeatability of the applied measurement method and is therefore not visible with this method.

4.2 | Nonelastic behavior of TZP-containing springs

The results of the deformation experiments prove a nonelastic behavior at room temperature of springs containing TZP. In the following section, we will compare and discuss the observations and explanatory models obtained on conventional TZP test bars described in the literature with our results on springs. We will consider the following aspects in turn: plastic deformation, influence of the deformation rate, deformation under constant load, and reversibility. Finally, by ruling out other approaches, we will highlight facilitated ionic displacement due to the presence of oxygen vacancies as the most likely mechanism for the anelasticity of TZP. At the end of the section, we will summarize the core arguments for this hypothesis.

In principle, nonelastic deformation can be caused by both anelastic and plastic processes. Plastic deformations at room temperature due to phase transformation and associated microcracking are considered the main causes of the excellent toughness of TZP materials. There are numerous publications that have investigated the transformation of the tetragonal to the monoclinic (t → m) phase in zirconia and the associated local volume expansion. An excellent overview is given by Chevalier et al.[20] However, literature and own experimental results and calculations argue against a martensitic phase transformation during spring deformation. First, the literature[21,22] reports that the critical stress level for the t → m transformation for commercially available 3Y-TZP materials is often close to their ultimate strength. Our calculations of the stress level in the ceramic springs during the deformation tests showed that the maximum shear stresses vary between 20 and 50 N/mm^2, depending on the spring material (Table 4). Thus, the shear stresses during compression of the springs are at least one order of magnitude smaller than the fracture stresses of the ceramic materials used. Second, the t → m phase transformation under mechanical load is a fast process. In contrast, we observed that spring deformation under constant load is not complete even after hours. Finally, complete resetting of the TZP springs was demonstrated. This would require a reconversion of the monoclinic to the tetragonal phase at room temperature. It can be concluded that the nonelastic spring deformation observed in the low stress range is exclusively due to anelasticity.

An anelastic behavior on 3Y-TZP was first demonstrated in the literature by Pan and Horibe[21–23] using strain gauges on flexural specimens. In a multitude of further experiments with similar experimental setup, the influence of stress intensity, deformation rate, and loading mode on the anelastic behavior of various TZP and PSZ materials was investigated by Matsuzawa and other scientists at Waseda University in Tokyo[24–30] in the following years. It was found that the anelastic characteristic affects phase transformation, crack growth, and ultimately the mechanical properties of TZP ceramics.

A comparison of our investigations on TZP springs stressed in shear with the literature on TZP specimens stressed in compression and tension reveals many similarities regarding the influence of the deformation rate, the deformation behavior at constant load, and the recovery after unloading.

4.2.1 | Influence of deformation rate

A significant dependence of the spring constant on the deformation rate was demonstrated for 3Y-TZP and 2Y-TZP. As the deformation rate increases, the spring constant increases. This means the springs become stiffer. For 3Y-TZP and 2Y-TZP springs, an almost identical rise of more than 3% was measured when the deformation rate was increased by two orders of magnitude (Table 5). For ATZ springs, an increase of only 1.3% was measured, even though only 15 wt.% Y-TZP was substituted by alumina in this material. For the significantly reduced anelasticity of ATZ compared to pure Y-TZP, it is probably also relevant that, according to the granule manufacturer,

not only yttria but also ceria was used to stabilize the TZP crystals (Table 1). For springs consisting of Ce-TZP only, an influence of the deformation rate on the spring constant could not be demonstrated. A pronounced effect of strain rate on room-temperature deformation[22] and crack growth[26,29] has been reported for 3Y-TZP under compression and tension stress. At low strain rate, 3Y-TZP was deformed significantly more than at high strain rate. In Ref. [24], the effect of strain rate on fracture strength was investigated on various zirconia materials in tensile test. For Y-TZP with submicron microstructure, the fracture strength increases with increasing strain rate. An analogous correlation was not found for Ce-TZP.

4.2.2 | Deformation under constant load

Y-TZP springs showed ongoing deformation under constant load in the tests, which was not completed even after 15 h. Although different deformation rates did not cause any change in the spring constant of Ce-TZP springs, a time-dependent deformation behavior was demonstrated for these springs under static loading. However, the absolute value of the nonelastic deformation of Ce-TZP springs is about one order of magnitude smaller than that of Y-TZP springs, as shown in Figure 4C. Similar differences in anelasticity were shown by 3Y-TZP and Ce-TZP bending specimens under constant load in a 4-point bending test rig,[27] provided that the stresses generated during the bending test were similarly low compared to the stresses generated when the spring was compressed. Under a bending stress of 100 MPa, the nonelastic deformation of the 3Y-TZP specimen was about 10 times higher than that of the Ce-TZP specimen.

4.2.3 | Reversibility

Measurements on Y-Ce-TZP springs show that their deformation is fully reversible after unloading. However, full spring relaxation is reached only after a few days. An analogous behavior is described in Ref. [27] for 3Y-TZP bending specimens. The deformation produced under bending load is also completely reversible, regardless of whether the specimens were loaded at 100 or 400 MPa. The recovery of the flexural specimens occurs over a period of 6–8 h, that is, faster than observed for springs. However, it cannot be excluded that these differences are due to the different sensitivities of the test methods used. For Ce-TZP flexural specimens, the extent of restraints was dependent on the level of previous loading. [27,28] After a low stress loading of 100 MPa, the resulting small deformation was completely reversible. Thus, the nonelastic deformation in this stress range is caused exclusively by anelastic processes. At a higher stress of 400 MPa, a much larger nonelastic strain was measured, caused by an additional plastic deformation, which was probably due to a martensitic phase transformation. The quantity of the anelastic deformation was independent of the level of the previous stress.

4.2.4 | Mechanism of anelastic deformation of TZP

Stress-induced grain rearrangement[22] and ferroelastic domain switching[22,31–34] were initially suggested as the cause of the anelasticity of TZP. Later, oxygen vacancies were proposed as a reason for anelasticity.[24,27,28] The latter theory is supported by the observed differences in the anelasticity of Y-TZP and Ce-TZP springs. If stabilizing ions with a valence different from that of Zr^{4+} are incorporated into the zirconia lattice, as is the case in Y-stabilized TZP materials by incorporating Y^{3+} ions, oxygen vacancies are created to maintain electroneutrality. In the case of Ce-TZP, the valences of the dopant cation Ce^{4+} and the matrix cation Zr^{4+} are the same, so that no vacancies are created in the matrix. It is suggested that the anelastic properties could be closely correlated with the overall level of oxygen vacancies in the matrix. The existence of oxygen vacancies should make a slight shift of the ions easier under an applied stress. This shift of ions allows the observed anelastic behavior.[28] Such mechanism based on short-range shift of ions is characterized by the saturation behavior of time-dependent strain, as observed in spring deformation experiments under constant load. This theory is also confirmed by the observation that a Ce-TZP with strongly pronounced anelastic behavior is obtained after thermal treatment in hydrogen.[25,28] In reducing atmosphere, cerium oxide is partially reduced, and additional oxygen vacancies are formed in the material.

Microstructure must also be discussed as another possible cause for the strongly different anelasticity of Y-TZP and Ce-TZP springs. Both the SEM images and the crystal size distributions provided in Figure S1 show that the crystals in the Y-TZP microstructures are significantly smaller than in the Ce-TZP microstructure. In addition, the 3Y-TZP microstructure is nearly monodisperse, whereas the Ce-TZP microstructure exhibits a broader crystal size distribution (Figure S2, Table S5). For nanostructured zirconia, nonelastic behavior at room temperature was observed in nanoindentation experiments.[35] The primary deformation mechanism is believed to be grain boundary sliding. This mechanism seems rather unlikely as an explanation for the deformation behavior of Y-TZP springs, as neither a nanocrystalline microstructure is present here nor

high stresses generated in nanoindentation experiments are reached in the spring tests.

4.2.5 | Summary

The findings on the deformation process of TZP springs can be summarized as follows: When the spring is compressed, a shear stress is generated in the ceramic. The magnitude of the shear stress varies across the coil cross section. Calculations show that the maximum shear stresses generated in the spring during the tests are much smaller than the fracture stresses of the TZP materials studied. As, according to the literature, the required transformation stress in 3Y-TZP is quite close to the fracture strength, the shear stress generated in the spring experiments is not reasonable enough to initiate a t → m phase transformation. Consequently, plastic deformation due to phase transformation and microcracking does not occur. This hypothesis is also strengthened by the finding that the nonelastic deformation is fully reversible. The observed deformation behavior of the TZP springs is thus determined exclusively by anelastic processes. These processes are most likely based on facilitated movement of ions in the crystal lattice due to the presence of oxygen vacancies. Intensity of anelastic spring deformation is influenced by absolute load, deformation rate, and type of stabilizing ions. Differences described in the literature between Y-TZP and Ce-TZP test specimens with respect to deformation under bending and tensile loading occur similarly under shear load in compressed helical springs. An experimental approach to measure the ion shift in TZP crystals could be an analysis of undeformed and deformed samples by total scattering or extended X-ray absorption fine structure.

5 | CONCLUSIONS

Ceramic helical springs with reproducible properties can preferably be produced by hard machining of hollow cylinders. Corresponding springs made of alumina, various TZP materials, and ATZ were presented. Due to the low tolerances of the spring dimensions and high surface quality, these springs permit a comparative, high-precision evaluation of the deformation behavior.

Only alumina springs showed linear elastic behavior in all deformation experiments. In contrast, time-dependent reversible deformation at room temperature was demonstrated on TZP and ATZ springs. The studies on the TZP springs confirm the influence of the stabilization component on the extent of anelasticity. The anelasticity is strongly pronounced in springs made of Y-TZP. Ce-TZP, on the other hand, exhibits very little anelastic deformation.

Oxygen vacancies in the TZP lattice are considered the most likely explanation for the anelasticity in TZP-containing springs. The presence of oxygen vacancies is thought to facilitate a slight displacement of ions under mechanical stress. Moreover, this theory offers a plausible explanation for the different behaviors of Y-TZP and Ce-TZP springs. When Y^{3+} ions are incorporated into the zirconia lattice, in contrast to the incorporation of Ce^{4+} ions, oxygen vacancies are formed in large numbers.

The final consequence of the deformation experiments is that only alumina springs can be used for a capacitive displacement sensor. TZP but also ATZ springs are unsuitable due to anelasticity already occurring at room temperature.

ACKNOWLEDGMENTS

The German Federal Ministry of Education and Research is thanked for the support of the research project "CERAFORCE" (grant number 13XP5006D). Thanks to our colleagues at BAM Bärbel Schulz for experimental work, Andreas Börner for spring manufacturing, Sigrid Benemann and Romeo Saliwan Neumann for electron microscopy, Paul Mrkwitschka for Feret analysis, Franziska Lindemann for granulometric measurements, Robert Mang for design of test devices, and Anna Meierfrankenfeld for measurement of spring deformation under constant load. Special thanks go to Carl Paulick from FHK Fügetechnik Hochleistungskeramik Eberswalde for creative ideas and intensive discussion.

ORCID

Björn Mieller https://orcid.org/0000-0002-0784-9790

REFERENCES

1. Harper CR. A ceramic spring for high-temperature valves. J Mater Energy Syst. 1979;1(2):62–7.
2. Sato S, Taguchi K, Adachi R, Nakatani M. A study on strength characteristics of Si3N4 coil springs. Fatigue Fract Eng Mater Struct. 1996;19(5):529–37.
3. Grujicic M, Galgalikar R, Snipes JS, Ramaswami S. Creep-behavior-based material selection for a clamping spring of ceramic-matrix composite inner-shroud in utility and industrial gas-turbine engines. Proc Inst Mech Eng Part L. 2018;232(5):388–402.
4. Hamilton T, Gopal M, Atchley E, Smith JE. Experimental investigation on the mechanical performance of helical ceramic springs. J Mater Sci. 2003;38(15):3331–5.
5. Chironis NP. Spring design and application. New York: McGraw-Hill; 1961. p. 86.
6. Buhl H, Weiss R. Carbon-fiber spring for high-temperature application. J Cryst Growth. 1993;131(3–4):470–2.
7. Kinoshita K, Yamada T. Spherical crystals of Pb1—xSnxTe grown in microgravity. J Cryst Growth. 1996;165(1):75–80.
8. Kaforey ML, Deeb CW, Matthiesen DH. Design of ceramic springs for use in semiconductor crystal growth in microgravity. J Cryst Growth. 2000;211(1–4):421–7.

9. Nohut S, Schneider GA. Failure probability of ceramic coil springs. J Eur Ceram Soc. 2009;29(6):1013–9.
10. Khader I, Koplin C, Schroder C, Stockmann J, Beckert W, Kunz W, et al. Characterization of a silicon nitride ceramic material for ceramic springs. J Eur Ceram Soc. 2020;40(10):3541–54.
11. Hayes MP, Morton P, Heinze R, Leistner H, Grievson B, Riley F. Development of advanced ceramic springs [Internet]. [cited 2023 Mar 15]. 17p. Available from: https://cordis.europa.eu/docs/projects/files/BRE/BRE20323/26840641-6_en.pdf
12. Krindges I, Andreola R, Perottoni CA, Zorzi JE. Low-pressure injection molding of ceramic springs. Int J Appl Ceram Technol. 2008;5(3):243–8.
13. Barbieri RA, Zorzi JE. Constante de mola de molas cerâmicas injetadas a baixa pressão. Cerâmica. 2011;57(344):381–6.
14. Barbieri RA, Perottoni CA, Zorzi JE. Influence of sintering temperature on the mechanical properties of alumina springs. Int J Appl Ceram Technol. 2012;9(3):599–605.
15. Kaya C, Butler E. Zirconia-toughened alumina ceramics of helical spring shape with improved properties from extruded sol-derived pastes. Scr Mater. 2003;48(4):359–64.
16. Chen S, Zhang Y, Zhang C, Xiong X, Li G, Hu H. A simple way to prepare C/SiC spring. Int J Appl Ceram Technol. 2014;11(1):186–92.
17. Nakao W, Mori S, Nakamura J, Takahashi K, Ando K, Yokouchi M. Self-crack-healing behavior of mullite/SiC particle/SiC whisker multi-composites and potential use for ceramic springs. J Am Ceram Soc. 2006;89(4):1352–7.
18. Zhuang MM, Wang MC, Zhao YN, Zheng B, Guo A, Liu JC. Fabrication and high-temperature properties of Y-TZP ceramic helical springs by a gel-casting process. Ceram Int. 2015;41(4):5421–8.
19. DIN e.V. Helical compression springs made of rectangular steel; Calculation. Berlin: Beuth-Verlag; 1971. 2p. Standard: DIN 2090:1971-01.
20. Chevalier J, Gremillard L, Virkar AV, Clarke DR. The tetragonal-monoclinic transformation in zirconia: lessons learned and future trends. J Am Ceram Soc. 2009;92(9):1901–20.
21. Pan LS, Horibe S. An in-situ investigation on the critical phase transformation stress of tetragonal zirconia polycrystalline ceramics. J Mater Sci. 1996;31(24):6523–7.
22. Pan LS, Horibe S. Anelastic behaviour of zirconia ceramics under monotonic and cyclic loadings. Acta Mater. 1997;45(2):463–9.
23. Pan LS, Imai N, Horibe S. Temperature dependence of anelastic behavior in 3Y-TZP ceramics. Mater Sci Eng: A. 1997;230(1–2):155–60.
24. Matsuzawa M, Abe M, Horibe S. Strain rate dependence of tensile behavior and environmental effect in zirconia ceramics. ISIJ Int. 2003;43(4):555–63.
25. Matsuzawa M, Abe M, Horibe S, Sakai J. The effect of reduction on the mechanical properties of CeO2 doped tetragonal zirconia ceramics. Acta Mater. 2004;52(6):1675–82.
26. Matsuzawa M, Horibe S. Resistance against crack nucleation and propagation inY(2)O(3) doped tetragonal zirconia ceramics. Mater Sci Eng: A. 2002;333(1–2):199–207.
27. Matsuzawa M, Horibe S. Analysis of non-elastic strain produced in zirconia ceramics. Mater Sci Eng: A. 2003;346(1–2):75–82.
28. Matsuzawa M, Horibe S, Sakai J. Anelasticity and strength in zirconia ceramics. KEM 2007;280–283:967–72.
29. Matsuzawa M, Sato F, Horibe S. The effect of anelasticity and phase transformation on crack growth in Y-TZP ceramics. J Mater Sci. 2001;36(10):2491–7.
30. Matsuzawa M, Yajima N, Horibe S. Damage accumulation caused by cyclic indentation in zirconia ceramics. J Mater Sci. 1999;34(21):5199–204.
31. Chan CJ, Lange FF, Ruhle M, Jue JF, Virkar AV. Ferroelastic domain switching in tetragonal zirconia single-crystals microstructural aspects. J Am Ceram Soc. 1991;74(4):807–13.
32. Virkar AV, Jan FJ, Smith P, Mehta K, Prettyman K. The role of ferroelasticity in toughening of brittle materials. Phase Transit. 1991;35(1):27–46.
33. Virkar AV, Matsumoto RLK. Ferroelastic domain switching as a toughening mechanism in tetragonal zirconia. J Am Ceram Soc. 1986;69(10):C224–6.
34. Foitzik A, Stadtwaldklenke M, Ruhle M. Ferroelasticity of t-ZrO2. Z Metallkde. 1993;84(6):397–404.
35. Liu E, Wang H, Xiao G, Yuan G, Shu X. Creep-related micromechanical behavior of zirconia-based ceramics investigated by nanoindentation. Ceram Int. 2015;41(10):12939–44.

SUPPORTING INFORMATION

Additional supporting information can be found online in the Supporting Information section at the end of this article.

How to cite this article: Rabe T, Kalinka G, Mieller B. Manufacturing and deformation behavior of alumina and zirconia helical springs at room temperature. J Am Ceram Soc. 2023;1–14. https://doi.org/10.1111/jace.19085